




## Article

# Impacts of the Tropical Cyclone Idai in Mozambique: A Multi-Temporal Landsat Satellite Imagery Analysis

Alberto Bento Charrua <sup>1,2,3</sup> , Rajchandar Padmanaban <sup>4</sup>, Pedro Cabral <sup>5</sup> , Salomão Bandeira <sup>6</sup> and Maria M. Romeiras <sup>1,\*</sup> 

- <sup>1</sup> Linking Landscape, Environment, Agriculture and Food (LEAF), Instituto Superior de Agronomia (ISA), Universidade de Lisboa, Tapada da Ajuda, 1349-017 Lisbon, Portugal; albecharrua@novasbe.pt
  - <sup>2</sup> Nova School of Business and Economics, Universidade Nova de Lisboa, Campus de Carcavelos, Rua da Holanda, n.1, Carcavelos, 2775-405 Cascais, Portugal
  - <sup>3</sup> Department of Earth Sciences and Environment, Faculty of Science and Technology, Licungo University, P.O. Box 2025, Beira 2100, Mozambique
  - <sup>4</sup> Forest Research Center (CEF), Instituto Superior de Agronomia (ISA), Universidade de Lisboa, Tapada da Ajuda, 1349-017 Lisbon, Portugal; rajchandar@isa.ulisboa.pt
  - <sup>5</sup> NOVA IMS, Universidade Nova de Lisboa, Campus de Campolide, 1070-312 Lisbon, Portugal; pcabral@novaims.unl.pt
  - <sup>6</sup> Department of Biological Sciences, Eduardo Mondlane University, P.O. Box 257, Maputo 1100, Mozambique; salomao.bandeira@uem.mz
- \* Correspondence: mmromeiras@isa.ulisboa.pt

**Abstract:** The Central Region of Mozambique (Sofala Province) bordering on the active cyclone area of the southwestern Indian Ocean has been particularly affected by climate hazards. The Cyclone Idai, which hit the region in March 2019 with strong winds causing extensive flooding and a massive loss of life, was the strongest recorded tropical cyclone in the Southern Hemisphere. The aim of this study was to use pre- and post-cyclone Idai Landsat satellite images to analyze temporal changes in Land Use and Land Cover (LULC) across the Sofala Province. Specifically, we aimed—(i) to quantify and map the changes in LULC between 2012 and 2019; (ii) to investigate the correlation between the distance to Idai’s trajectory and the degree of vegetation damage, and (iii) to determine the damage caused by Idai on different LULC. We used Landsat 7 and 8 images (with 30 m resolution) taken during the month of April for the 8-year period. The April Average Normalized Difference Vegetation Index (NDVI) over the aforementioned period (2012–2018, pre-cyclone) was compared with the values of April 2019 (post-cyclone). The results showed a decreasing trend of the productivity (NDVI 0.5 to 0.8) and an abrupt decrease after the cyclone. The most devastated land use classes were dense vegetation (decreased by 59%), followed by wetland vegetation (–57%) and shrub land (–56%). The least damaged areas were barren land (–23%), barren vegetation (–27%), and grassland and dambos (–27%). The Northeastern, Central and Southern regions of Sofala were the most devastated areas. The Pearson Correlation Coefficient between the relative vegetation change activity after Idai (NDVI%) and the distance to Idai’s trajectory was 0.95 (R-square 0.91), suggesting a strong positive linear correlation. Our study also indicated that the LULC type (vegetation physiognomy) might have influenced the degree of LULC damage. This study provides new insights for the management and conservation of natural habitats threatened by climate hazards and human factors and might accelerate ongoing recovery processes in the Sofala Province.



**Citation:** Charrua, A.B.; Padmanaban, R.; Cabral, P.; Bandeira, S.; Romeiras, M.M. Impacts of the Tropical Cyclone Idai in Mozambique: A Multi-Temporal Landsat Satellite Imagery Analysis. *Remote Sens.* **2021**, *13*, 201. <https://doi.org/10.3390/rs13020201>

Received: 26 November 2020

Accepted: 6 January 2021

Published: 8 January 2021

**Publisher’s Note:** MDPI stays neutral with regard to jurisdictional claims in published maps and institutional affiliations.



**Copyright:** © 2021 by the authors. Licensee MDPI, Basel, Switzerland. This article is an open access article distributed under the terms and conditions of the Creative Commons Attribution (CC BY) license (<https://creativecommons.org/licenses/by/4.0/>).

**Keywords:** Cyclone Idai; remote sensing; vegetation damage; land use and land cover; vegetation index

## 1. Introduction

Tropical cyclones are among the most devastating natural disasters owing to their great potential for loss of human life, significant economic decline and severe environmental damage [1–3]. The Southwestern Indian Ocean is one of the main tropical cyclone areas

in the world [4], and also the most cyclone active area in the Southern Hemisphere [5]. Currently, the negative effects of climate change are an omnipresent reality in Mozambique, as this southern African country frequently experiences extreme weather and climate events such as drought, floods and cyclones [6]. The cyclone season in Mozambique generally spans the period of November to April. Every year, three to twelve cyclones form in the Mozambique Channel [7,8]. The Central region of Mozambique, including the Sofala Province, is the area most prone to cyclones (six cyclones in 16 years) and climate hazards. This region is characterized by a large tidal range (up to 7 m), and extensive low flatland [9–11]. The most severe tropical cyclones striking Sofala and affecting the lives of millions of inhabitants were—Nadia in 1994, Bonita in 1996, Lisete in 1997, Eline in 2000, Japhete in 2003, and Idai in March 2019 [12,13]. Idai (category four) was the most devastating and deadliest cyclone recorded in the Southern Hemisphere, in terms of the loss of human life, of facilities and of infrastructures [14,15]. Idai primarily affected Sofala and impacted the surrounding provinces (Manica, Inhambane, Tete and Zambézia), while also wreaking havoc in Zimbabwe as well. It brought torrential rain (more than 200 mm in 24 h) and strong winds (up to 220 km/h), causing severe widespread flooding (flood waters rose more than 10 m). Idai affected more than 1.5 million people in Mozambique, resulting in more than 600 deaths while over 1600 persons were injured. However, severe Land Use and Land Cover (LULC) damage has not yet been fully quantified. Cyclone Idai's socioeconomic impact in Mozambique was considered the highest to date, with damages and losses estimated at US \$3.2 billion (2019 estimate) [12].

Several studies using satellite images to assess the impact of cyclones on natural habitats have been reported from different parts of the world, including the USA [16], the Gulf of Mexico and Caribbean/Mesoamerican Region [17], Australia [18], and India and Bangladesh [19]. In Africa and Mozambique in particular, cyclone impact studies on LULC are comparatively rare.

The Sofala Province is an under-researched area. With the exception of two studies carried out on the Save River Delta (forming the border between South and Central Mozambique), which assessed the response of mangroves to cyclone Eline (2000) using SPOT images [20], and the qualitative analysis of natural system management under recurrent catastrophic events (cyclones and floods) [21], no published reports have been detected. Our study is the first to document the impact of the category four Cyclone Idai on LULC.

Studying the impact of cyclones on LULC in the context of climate change is crucial to inform the design and implementation of natural vegetation management, identify threatened habitats, prevent and/or counter environmental threats, and enhance conservation efforts. Moreover, our study provides valuable information for evidence-based decision making and disaster management for a more effective recovery of both natural habitats and human infrastructures in the Sofala Province. It also gives relevant insights into the sensitivity and recovery of natural vegetation following a devastating cyclone. Since Idai damaged communication and transport networks, as well as other basic infrastructures, traditional field work to survey the large-scale destruction of vegetation is difficult, expensive and time-consuming when compared to remote sensing [22–24].

Vegetation indicators, including the Normalized Difference Vegetation Index (NDVI) and the Enhanced Vegetation Index, have been widely used to obtain useful information on vegetation destruction and sensitivity, particularly after a damage event [24–26]. Landsat data images are easy to access, and have long been used to monitor land use and changes in vegetation cover [27–29]. Therefore, the main purpose of this study was to use pre- and post-Idai Landsat imagery to analyze temporal changes in Sofala's LULC from 2012 to 2019. Specifically, we aimed—(i) to quantify and map LULC dynamics from 2012 to 2019; (ii) to investigate how the distance to Idai's trajectory related to vegetation damage, and (iii) to determine the degree of damage caused by the cyclone on different LULC classes. The findings of this study are meant to assist managers of natural resources to design and implement efficient strategies and practices in order to safeguard natural ecosystems

and their services such as provisioning (e.g., food, and timber), regulating (e.g., climate regulation, and water purification), supporting (e.g., nutrient cycling, and soil formation), and cultural (recreation, and spiritual) [30].

## 2. Materials and Methods

### 2.1. Study Area

Sofala is a coastal province in Central Mozambique, occupying a surface area of approximately 68,018 km<sup>2</sup> (about 8.5% of the country). It borders on the Indian Ocean to the east, on the Zambezi River to the north, and the Save River to the south (Figure 1a). The Central part of Sofala is intersected by the Púnguè and the Buzi River, and the province is characterized by an inter-connected hydrological system of creeks, swamps, and lakes. All the region's main rivers discharge into the Indian Ocean, providing a suitable habitat for the growth and establishment of a great variety animal and plant species. According to the 2017 census, the total population of Sofala province was estimated at 2,259,248 inhabitants, most of them living in rural areas [31] and largely dependent on unstable natural resources (threatened by climate hazards) for their subsistence. The main economic activities of the local population are slash and burn agriculture, fishing, raising cattle and commerce. The Province of Sofala is characterized by a tropical climate with rainy season (summer) running from November to March, and a dry season (winter) from April to October; southeasterly trade winds are predominant. The annual average temperature is 25 °C and average rainfall amounts to approximately 1300 mm/year [32]. According to Marzoli [33], LULC classes in Sofala are primarily composed of vast native forests (48.81%), wetlands (19%), agricultural lands (5.57%), urban areas (0.16%), barren areas (0.5%), with water and other vegetation formations (height < 5 m) accounting for 25.96%. Sofala's coastline is characterized by the so-called swamp coast [34] and it has one of the largest mangrove areas (932 km<sup>2</sup>) in Mozambique, second only to the Zambezia province (1219 km<sup>2</sup>) [33]. Sofala is the province most prone to floods and cyclones (occurring in summer) which greatly affect LULC [9,11].

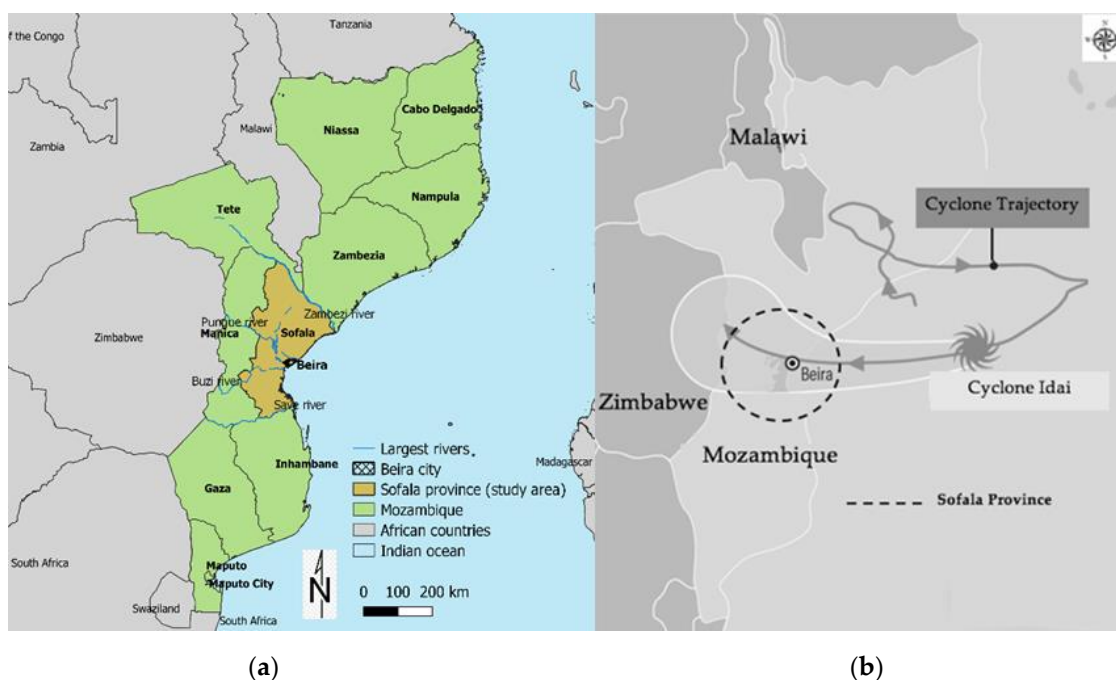


**Figure 1.** Location of the study area (a) and trajectory of Cyclone Idai (b) (adapted from Meteo France).

## 2.2. The Cyclone IDAI

Cyclone Idai originated from a tropical depression that formed in the Mozambique Channel on 4 March 2019. On 9 March, the depression intensified, transforming it into the, as yet, moderate tropical storm Idai. The reigning conditions in the Mozambique Channel greatly favored the intensification of the winds to speeds of 175 km/h on 11 March. Idai then weakened and died down for a day, only to re-activate on 13 March. On the night of 14 to 15 March, Idai turned into a category four tropical cyclone making landfall near Beira, the main city in Central Sofala, Mozambique's second largest city, and a strategic maritime port which serves Mozambique's interior as well as a vast southern African hinterland region (e.g., Zimbabwe, Botswana, Malawi, Zambia, and Democratic Republic of Congo) (Figure 1b). It brought strong winds (180–220 km/h) and torrential rain (more than 200 mm in 24 h), flooding more than 3000 km<sup>2</sup> of agricultural land. It displaced around 400,000 inhabitants, provoking over 600 deaths, while severely damaging LULC classes [12]. The winds receded as the cyclone moved inland, affecting provinces bordering on Sofala (Manica, Zambézia, Tete, and Inhambane) before moving to neighboring Zimbabwe.

## 2.3. Data

We used Landsat 7 Enhanced Thematic Mapper Plus (ETM+) and Landsat 8 Operational Land Imager (OLI) images from April of each year, from 2012 to 2015, and 2016 to 2019, respectively. Landsat 7 ETM+ and Landsat 8 OLI data both had a 30 m resolution and were downloaded from the United States Geological Survey (USGS) gateway (<https://earthexplorer.usgs.gov/>). Table 1 shows the list of satellite images used, acquisition date, and path row for the study area. The LULC and NDVI analyses can be influenced by seasonal differences (because of changes in atmospheric conditions and photosynthetic activities) [35].

**Table 1.** Satellite imagery used in this study.

Date	Sensor	Path Row
12 April 2012	Landsat 7 ETM+	166/73
19 April 2012	Landsat 7 ETM+	167/72, 73, 74, 75
28 April 2012	Landsat 7 ETM+	168/72, 73, 74
13 April 2013	Landsat 7 ETM+	166/73
15 April 2013	Landsat 7 ETM+	167/72, 73, 74, 75
22 April 2013	Landsat 7 ETM+	168/72, 73, 74
2 April 2014	Landsat 7 ETM+	166/73
16 April 2014	Landsat 7 ETM+	167/72, 73, 74, 75
18 April 2014	Landsat 7 ETM+	168/72, 73, 74
12 April 2015	Landsat 7 ETM+	166/73
12 April 2015	Landsat 7 ETM+	167/72, 73, 74, 75
19 April 2015	Landsat 7 ETM+	168/72, 73, 74
6 April 2016	Landsat 8 OLI	166/73
13 April 2016	Landsat 8 OLI	167/72, 73, 74, 75
29 April 2016	Landsat 8 OLI	168/72, 73, 74
9 April 2017	Landsat 8 OLI	166/73
16 April 2017	Landsat 8 OLI	167/72, 73, 74, 75
25 April 2017	Landsat 8 OLI	168/72, 73, 74
12 April 2018	Landsat 8 OLI	166/73
19 April 2018	Landsat 8 OLI	167/72, 73, 74, 75
28 April 2018	Landsat 8 OLI	168/72, 73, 74
6 April 2019	Landsat 8 OLI	166/73
15 April 2019	Landsat 8 OLI	167/72, 73, 74, 75
22 April 2019	Landsat 8 OLI	168/72, 73, 74

## 2.4. Methods

This study was carried out in four main steps—(1) satellite data pre-processing, which included cloud detection, atmospheric correction, and geometric correction; (2) calculation

of the vegetation indicators, including the Normalized Difference Vegetation Index (NDVI), the difference in NDVI ( $\Delta$ NDVI), and the relative change in vegetation productivity after Idai (NDVI%); (3) producing the LULC map for April 2019; and (4) producing a distance bands map obtained using buffer analysis. These steps are detailed in Figure 2. The distance to the cyclone's trajectory was subjected to statistical analyses to evaluate its relationship with vegetation damage using a linear regression model with a single explanatory variable.

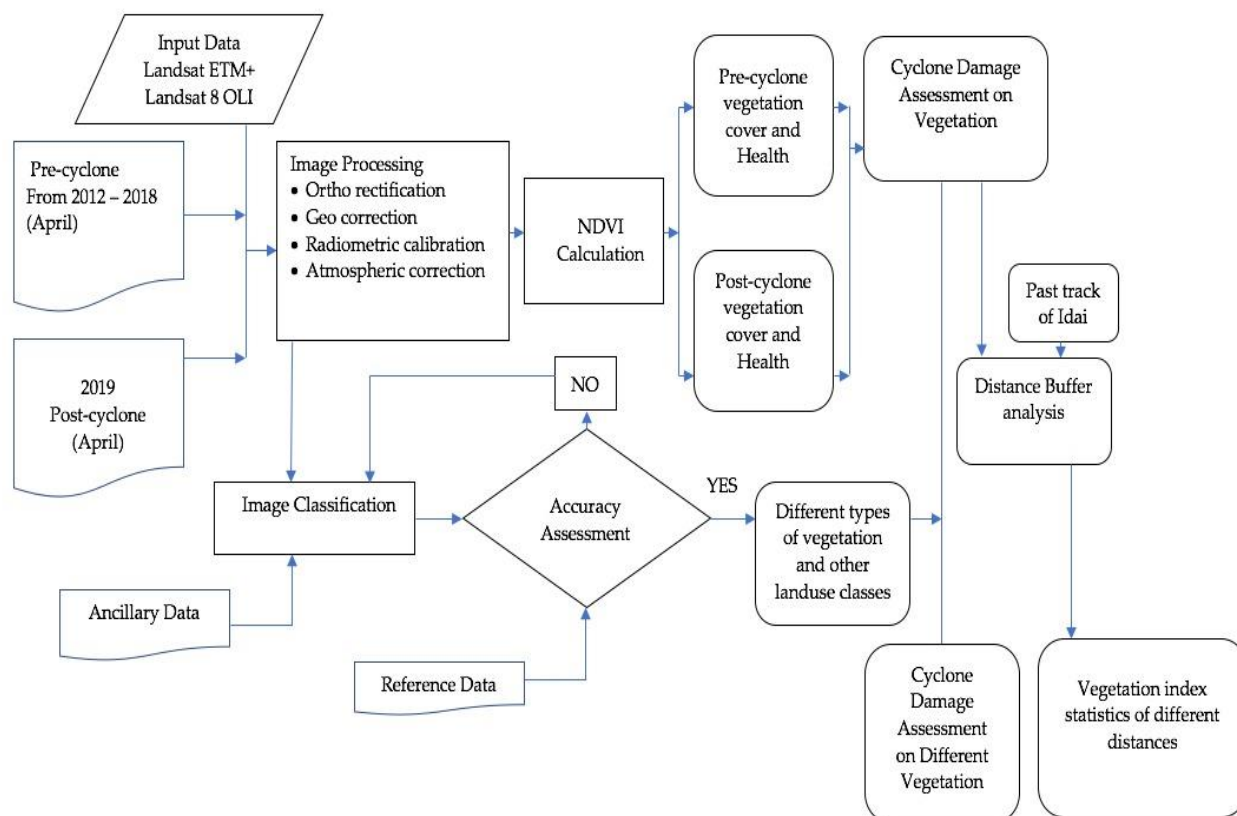


**Figure 2.** Workflow of Land Use and Land Cover (LULC) classification.

Initially, the Landsat 7 and 8 satellite data were geometrically corrected and orthorectified (Figure 2) using the Landsat packages (“georef” and “geoshift”) in RStudio Software [36–38]. All satellite images were georeferenced through the Universal Transverse Mercator (UTM) coordinate system. We were aware of the limitation of Landsat 7 ETM+ because of the Scan Line Corrector (SLC) failure [39,40]. To fill the gaps (Not available “NA” values) caused by that error, we applied the Landsat 7 Scan Line Corrector (SLC)-off Gap function, using the traditional Local Linear Histogram Matching method—LLHM [37,41]. The ERDAS image processing software (version 8.7) was applied to perform Scan line error correction with the help of band-specific gap mask files, made with the Landsat 7 Level-1 data product. These mask files help to classify the location of every pixel affected by the original data gaps in the primary SLC-off scene [36]. For this purpose, the DV values (0–255) were converted into top-of-atmosphere (TOA) radiance (at-satellite radiance values) using the parameters provided in metadata files [38,42,43]. We also applied absolute atmospheric compensation techniques (Dark Object and Modified Dark Object Subtraction Method) to identify and remove clouds, aerosols, and cirri [36,44].

The pseudo-invariant features (PIF) function was used to examine the homogeneity of reflectance values of LULC in the images, and then corrected by using major axis regression. The Landsat 7 and 8 data were radiometrically and atmospherically corrected by using an atmospheric simulation model available in the Landsat and R package (RStoolBox) [38,45].



### 2.5. Land Use and Land Cover Classification

The satellite images for 2019 were classified into nine LULC classes—dense vegetation, shrub land, grassland and dambos, agricultural land, wetland vegetation, barren vegetation, barren land, built-up areas, and water bodies (Table 2). This was performed by applying the Random Forest (RF) classifier. This technique has been recently used for mapping plant species and landscape due to its processing speed, improved accuracy, and reliable classification outputs [46,47]. The processing chain for the RF classification algorithm optimized the proximities between data points [48]:

- Produces n-tree bootstrap model from the raster data;
- Runs an unpruned classification grown for all bootstrap models according to the DN values;
- Produces N number of polygons in line with the DN raster values;
- Chooses the number of classifications of the LULC classes; and
- Illustrates LULC classification.

For the LULC classification, we used “randomForest” packages [49] in the open-source RStudio software version 1.3.1073 [50]. Furthermore, the packages Classes and Methods for Spatial Data (Sp) [51], raster [52], and Raster Geospatial Data Abstraction Library (Rgdal) [53] were used to process and visualize the spatial data.

**Table 2.** Land use and land cover types identified for the Sofala Province.

ID	Land Use and Land Cover Types	Description
1	Dense Vegetation	Woodland and forest
2	Shrub land	Brush, scrubland, shrubs and bush
3	Grassland and dambos	Grasses, rush and sedge
4	Agricultural land	Pasture, crop cultivation area, hay and other fruit plants
5	Wetland vegetation	Coastal and marine ecosystems including swamps, saltmarshes, and mangroves
6	Barren vegetation	Stunted, sparse and limited vegetation form/structure
7	Barren land	Sand, rocks, dry salt flats (including salt pans), mines, gravel pits and quarries
8	Built-up areas	Settlements, roads, bridges, urban and other infrastructures
9	Waterbodies	River, open water, lakes, streams, estuaries and ponds

### 2.6. Accuracy Assessment

The accuracy assessment is a widely applied technique to quantify how close the result of land cover classification is to the reference image. In this study, the accuracy was assessed by comparing the results of the obtained LULC map (classified image) with reference Google Earth images retrieved from the Google Earth Engine (GEE) [54] for the year 2019. From the classified LULC, seventy-five random point samples were produced for the study period. They were visually distinguished from GEE by comparison with the classified map. A confusion matrix was constructed to assess accuracy [48]. The quantitative accuracy assessment of the classified map was obtained by calculating the kappa coefficient (k) using ERDAS Imagine (version 8.7) [55]. The model’s accuracy is classified according to k values as follows—poor ( $k < 0.2$ ), moderate ( $0.4 < k < 0.6$ ) and near perfect ( $k > 0.8$ ) (see Jensen [35] and Louarn et al. [47], for further detail).

## 2.7. Vegetation Indices

The Normalized Difference Vegetation Index (NDVI) is generally used to measure vegetation density and its health status (level of photosynthetic activity) and is less affected by topographic factors and illumination [24]. The NDVI is calculated as follows:

$$NDVI = \frac{(NIR - RED)}{(NIR + RED)}, \quad (1)$$

where NIR and RED are the spectral reflectances corresponding to the fourth (0.77–0.90  $\mu\text{m}$ ) and third (0.63–0.69  $\mu\text{m}$ ) Landsat ETM+ bands, respectively [24]. For Landsat 8 OLI, NIR is the fifth band (0.85–0.88  $\mu\text{m}$ ) and RED is the fourth band (0.64–0.67  $\mu\text{m}$ ) [23]. Normally, NDVI ranges between  $-1.0$  and  $1.0$  with vegetation land covers ranging from  $0.0$  to  $1.0$ . The difference in NDVI (hereafter referred to as  $\Delta\text{NDVI}$ ) can show the change in LULC, while a negative  $\Delta\text{NDVI}$  represents the vegetation damage caused by Cyclone Idai. It is calculated by subtracting the NDVI image of one date (after) from that of another (before) using map algebra, which is a cell-by-cell process [24,56]. In this study, the Average NDVI in April over the 7-year period (2012–2018) represents the situation before Cyclone Idai (hereafter referred as pre-cyclone) whereas the NDVI of April 2019 represents the post-cyclone situation (hereafter referred as post-cyclone). The  $\Delta\text{NDVI}$  is calculated using the following equation:

$$\Delta\text{NDVI} = \text{NDVI}_{\text{post}} - \text{NDVI}_{\text{pre}}, \quad (2)$$

where  $\text{NDVI}_{\text{pre}}$  and  $\text{NDVI}_{\text{post}}$  are NDVI before and after cyclone, respectively. We also calculated the relative vegetation change activity after Idai ( $\text{NDVI}\%$ ) by using the equation below:

$$\text{NDVI}\% = \frac{\Delta\text{NDVI}}{\text{NDVI}_{\text{pre}}} \times 100 \quad (3)$$

Please note that a higher  $\text{NDVI}\%$  indicates lower damage. We used Sp [51], raster [52], rts [57], and Rgdal [53] packages in R studio for calculation of NDVI and the changes in vegetation productivity.

## 2.8. Distance to the Cyclone Trajectory

A distance map based on the Cyclone Idai's track was produced with distance bands calculated using ArcGIS (ESRI, 2020); 10 multiple buffers at the specified distance of 25 km from the best track line were obtained [23].

## 2.9. Correlation Analysis

We used the Pearson Correlation Coefficient to assess the relationship between vegetation damage and the distance to the cyclone's trajectory. This relationship was measured by means of a least squares estimator from the linear regression model with a single influencing/explanatory variable [23,24].

## 3. Results

### 3.1. Land Use and Land Cover

Figure 3 displays the nine LULC classes obtained for the Sofala Province. The kappa coefficient ( $>0.80$ ) (Table 3) shows a high accuracy level, indicating a good agreement between the LULC map for April 2019 and ground-truth based on GEE images [35,47]. Table 3 shows that the Producer's accuracy (i.e., how often are real features on the ground correctly shown on the LULC map) and user's accuracy (i.e., how often the class on the LULC map will actually be present on the ground) presented different values for each class, with a much higher accuracy for barren vegetation (PA: 92.5; UA: 94.1) [58].

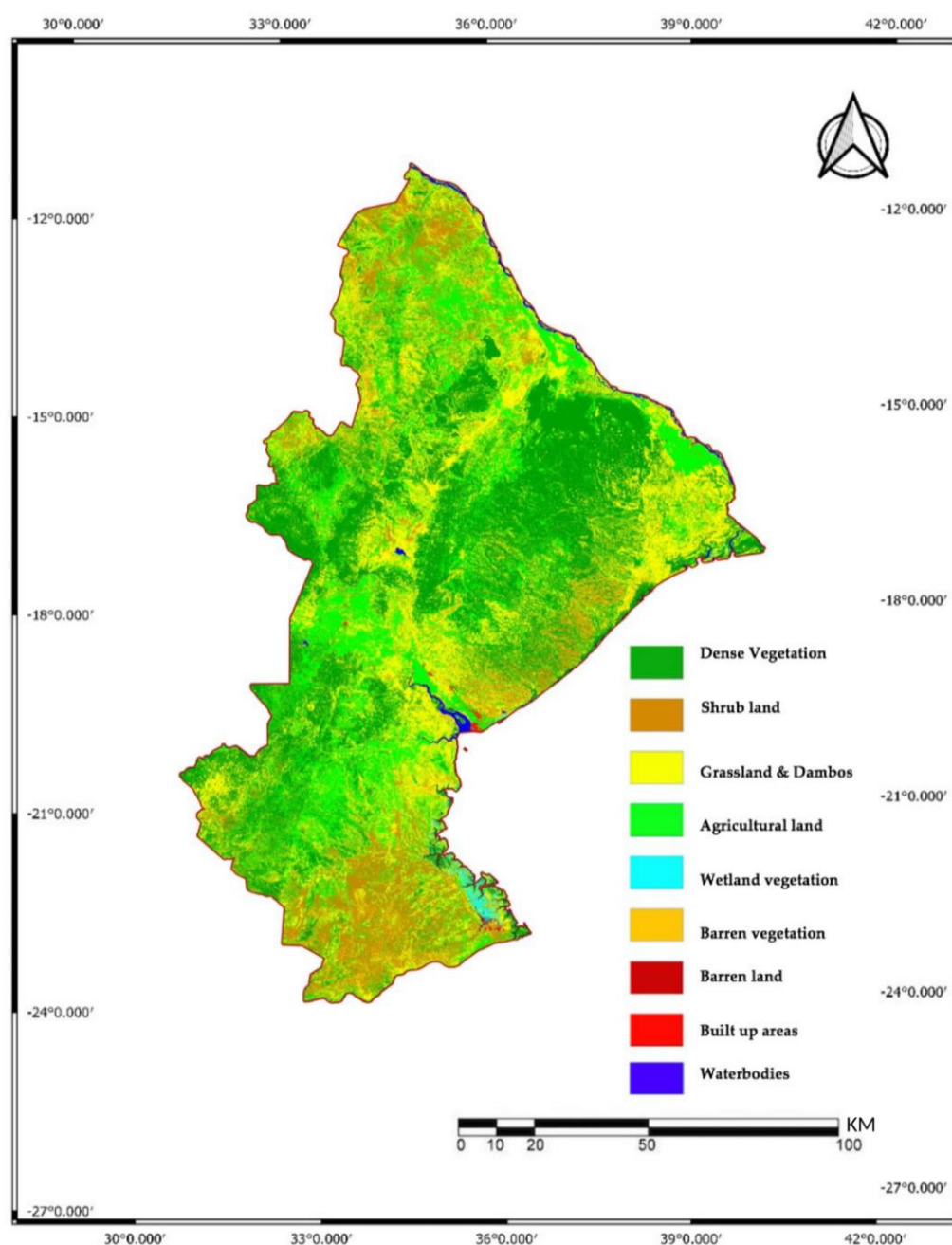


**Figure 3.** Land cover map of the Sofala Province in April 2019.

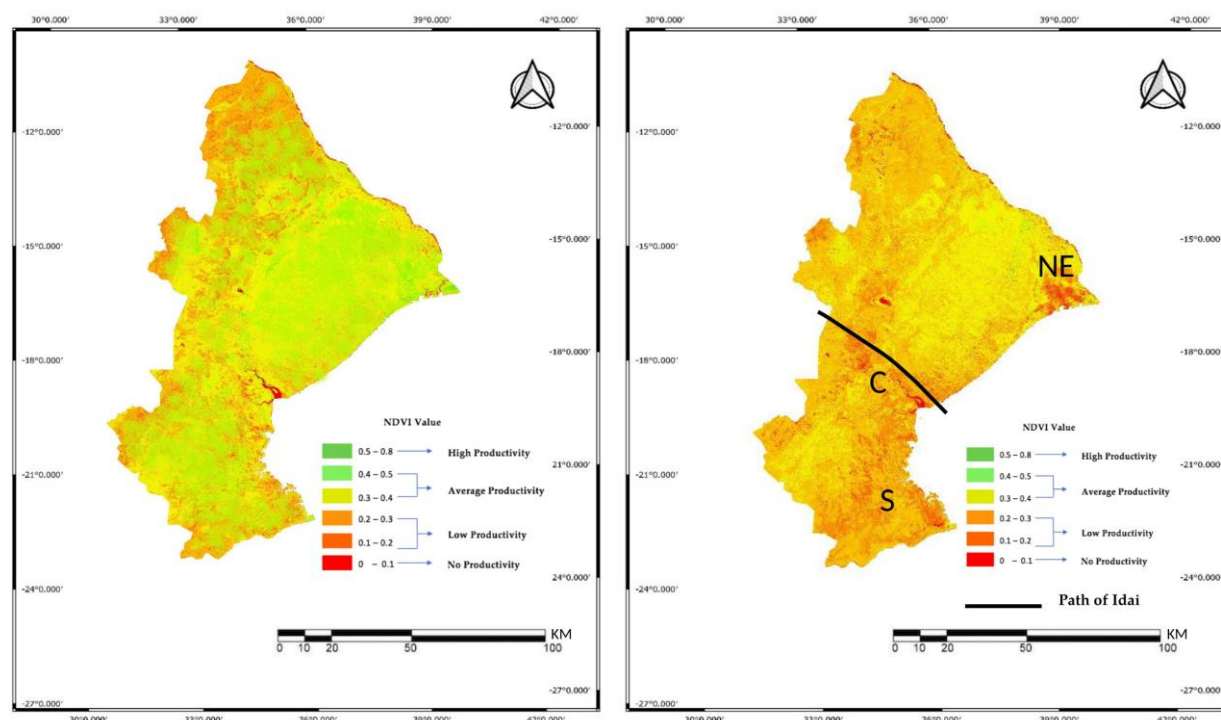
**Table 3.** The confusion matrix of the LULC map.

LULC Types	Producer Accuracy	User Accuracy
Dense vegetation	83.6	91.6
Shrub land	81.2	83.6
Grassland and dambos	89.9	92.7
Agriculture land	87.1	89.3
Wetland vegetation	88.3	92.4
Barren vegetation	92.5	94.1
Barren land	87.7	89.3
Built-up areas	80.6	84.2
Waterbodies	86.4	86.4



### 3.2. NDVI

Figure 4 illustrates the spatial distribution of pre-cyclone (left) and post-cyclone (right) NDVI. The comparison by optical remote sensing shows the loss of green leaves on the post-cyclone imagery, as indicated by the increase of no productivity and/or low productivity pixels [23,24]. Significant NDVI alterations were observed across the entire Province, with the largest LULC changes detected in the Northeast (NE), Central (C), and Southern (S) regions.



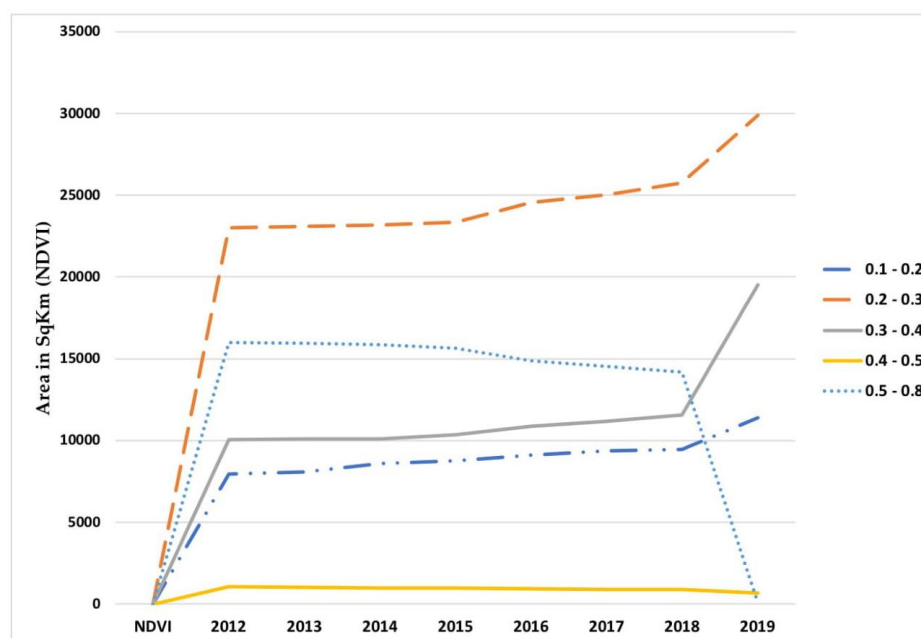
**Figure 4.** Spatial distribution of April Normalized Difference Vegetation Index (NDVI) averages in the Sofala Province. Pre-cyclone (left: Average NDVI over 7 years (2012–2018), and post-cyclone (right: 2019). NE—Northeastern, C—Central, and Southern (S) regions of the Province.

Table 4 shows the land cover classes affected by the Cyclone Idai. All post-cyclone images were acquired within three or four weeks of Idai's passage through the Sofala Province, i.e., before the damaged vegetation had recovered. The  $\Delta$ NDVI ranged from  $-0.07$  to  $-0.46$ ; the highest damage was found for dense vegetation ( $-58.9\%$ ), wetland vegetation ( $-57.4\%$ ), and shrub land ( $-55.5\%$ ); the least damage was observed in barren land ( $-22.5\%$ ), barren vegetation ( $-26.9\%$ ), and grassland and dambos ( $-27.1\%$ ).

**Table 4.** Land cover classes affected by the cyclone (pre-cyclone—average April NDVI over 2012–2018; after-cyclone—April 2019).

Land Cover Types	Counts (Pixels)	Total Area (SqKm)	Mean NDVI Pre-Cyclone	Mean NDVI Post-Cyclone	$\Delta$ NDVI	NDVI%
Dense vegetation	45,393,777	40,854.4	0.78	0.32	$-0.46$	$-58.9$
Shrub land	1,1070,577	9963.52	0.63	0.28	$-0.35$	$-55.5$
Grassland and dambos	3,980,911	3582.82	0.59	0.43	$-0.16$	$-27.1$
Agriculture land	5,705,377	5134.84	0.66	0.45	$-0.21$	$-31.8$
Wetland vegetation	8,104,666	7294.20	0.54	0.23	$-0.31$	$-57.4$
Barren vegetation	23,711	21.34	0.52	0.38	$-0.14$	$-26.9$
Barren land	399,033	359.13	0.31	0.24	$-0.07$	$-22.5$
Built-up areas	42,977	38.68	0.28	0.19	$-0.09$	$-32.1$

Figure 5 clearly shows an abrupt decrease of the area of highly productive vegetation classes (0.5–0.8) in April 2019, associated with a substantial growth of the low productivity vegetation area. Overall, almost all the highly productive vegetation experienced a severe decrease (over 99%) while the areas with low productivity vegetation increased by 22–80% as shown in the inset table of Figure 5.



Vegetation Productivity Classes	NDVI Values	Mean Pre-Cyclone	Post-Cyclone	Changes in Area Coverage	
				SqKm	%
Low Productivity	0.1 – 0.2	9059.24	11375.1	2315.86	25.56
	0.2 – 0.3	24379.22	29882.1	5502.88	22.57
Moderate	0.3 – 0.4	10811.26	19510.2	8698.94	80.46
Productivity	0.4 – 0.5	936.78	672.08	- 264.7	- 28.26
High Productivity	0.5 – 0.8	15016.54	72.20	- 14944.34	- 99.52

**Figure 5.** The time series of average of April NDVI from 2012 to 2019. Low Productivity—0.1–0.2 and 0.2–0.3, Moderate Productivity—0.3–0.4 and 0.4–0.5, and High Productivity—0.5–0.8. The inset table shows vegetation productivity changes (pre-cyclone vs. post-cyclone).

### 3.3. Influence of the Distance to the Cyclone Trajectory

The distance to the Cyclone Idai trajectory map is shown in Figure 6 for Sofala Province. The NDVI% was calculated for each distance class (Table 5). NDVI% increased with the distance from the cyclone trajectory (Figure 7 and Table 5).

**Table 5.** Values of the vegetation indices changes at different distances from the cyclone trajectory.

Distance (km)	Counts (Pixels)	ΔNDVI	NDVI%
0–25	7,516,910	−0.38	−55.07
25–50	8,079,493	−0.32	−53.3
50–75	8,605,728	−0.36	−52.9
75–100	8,768,752	−0.25	−45.4
100–125	10,234,104	−0.19	−30.1
125–150	10,724,540	−0.13	−26.5
150–175	8,988,106	−0.15	−26.3
175–200	5,451,298	−0.13	−25.01
200–225	3,909,496	−0.11	−21.5
225–250	3,003,413	−0.12	−18.4

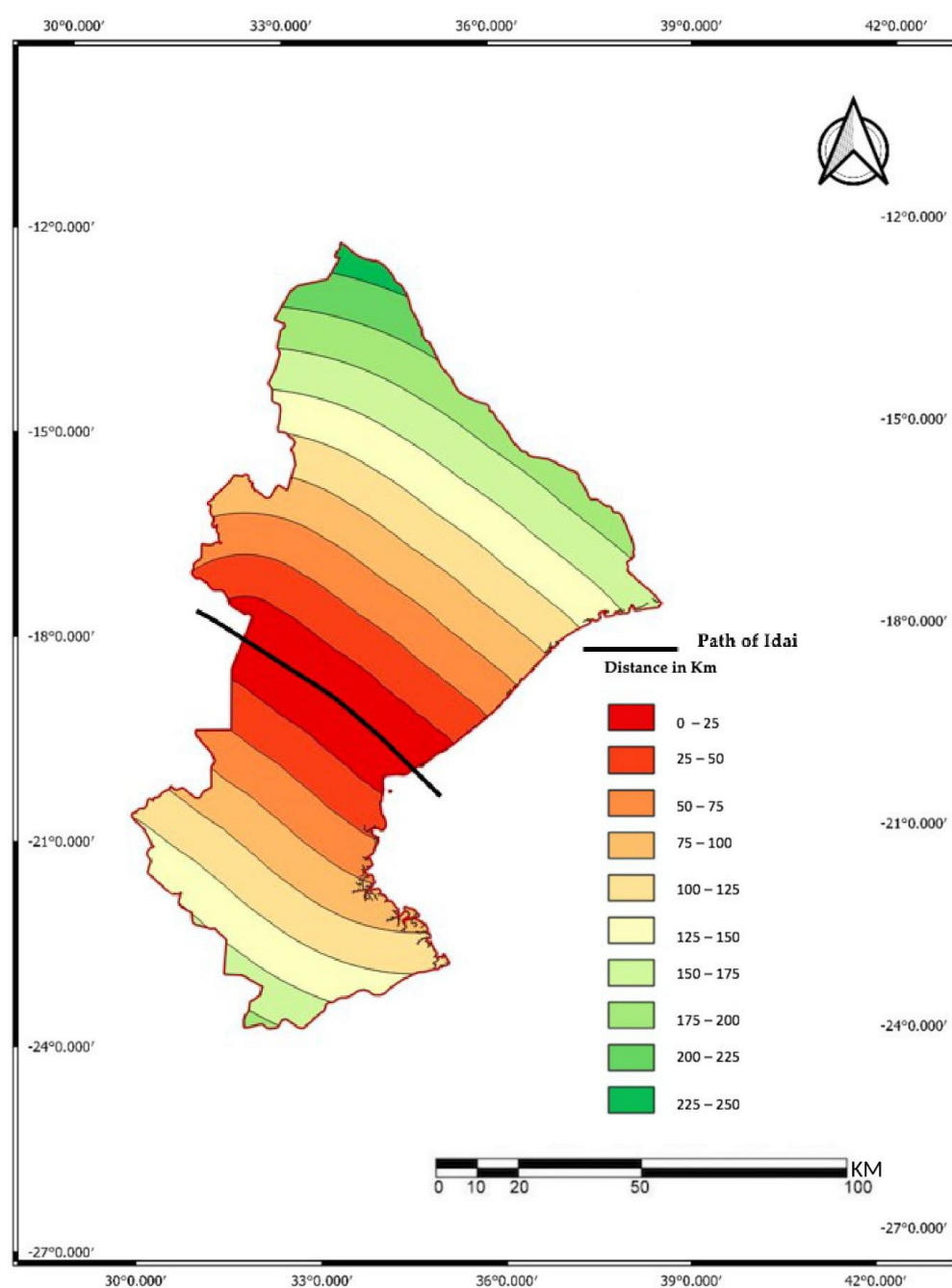


**Figure 6.** The Distance bands map (km) of Sofala Province.

At distances shorter than 75 km from the cyclone trajectory, land degradation was higher than 50% in NDVI. Even at distances over 200 km, NDVI was still above 20% (Figure 7 and Table 5).

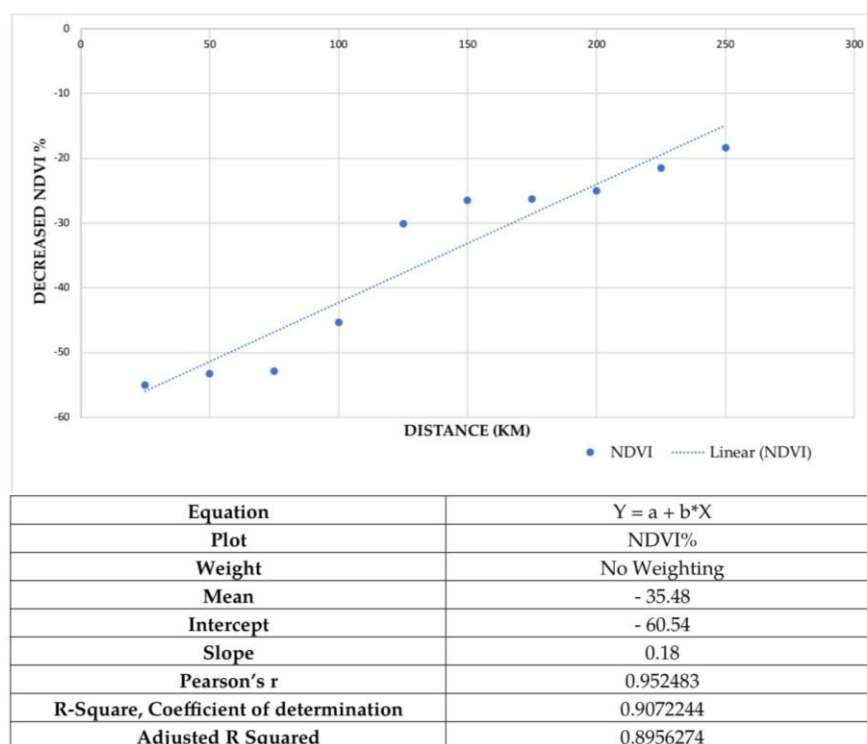


**Figure 7.** Pearson's correlation between mean NDVI% and distance to the Idai's trajectory.

## 4. Discussion

### 4.1. The Changes in NDVI

The vegetation productivity changes from 2012 to 2019 were quantified (Figure 5). In general, the areas with no productivity and/or low productivity tended to increase with time and an abrupt increase was observed in April 2019 (post-cyclone), whereas the high productivity pixels showed an opposite trend. The loss of vegetation productivity with time is a great concern globally and, most particularly, in low-income countries like Mozambique prone to climatic hazards. Mozambican forests and other natural ecosystems are under greater anthropogenic pressure (e.g., slash and burn agriculture, timber for building local infrastructures, firewood, and charcoal production, and urban expansion) while being adversely affected by natural factors (e.g., climate hazards, rising sea levels and frequent flooding) [11,59,60]. The category four tropical Cyclone Idai was the most devastating and deadliest ever recorded in the Southern Hemisphere. It brought strong winds and torrential rains, causing extensive flooding and leaving many communities in the Sofala Province submerged under 10 m of water [61]. It also caused a loss of 99.5% of high-productivity vegetation and an increment of up to 80.5% of the low- and moderate-productivity areas (Figure 5).

NDVI clearly changed over the whole Sofala Province after Idai's passage. The North-eastern, Central, and Southern regions (Figure 4) appear to be the most devastated areas. At "NE" a high concentration of the pixels of no productivity and/or low productivity region is clearly visible, where our results show the predominance of dense vegetation, agricultural area and water courses with regularly flooded wood and/or herbaceous species (Figures 3 and 4) [62]. Our findings are in line with Couto et al. [63] and Ramsar [64] who described this Northeastern region as part of the Ramsar site of the Zambezi Delta and of the Marromeu Complex, which are designated Wetlands of International Importance (conservation hotspot). This region is characterized by a broad flat alluvial area with a rich mosaic of grassland and dambos, woodland, thicket, large water swamps, and an extensive area covered in mangrove. The devastation in Central Sofala Province is closely related to Idai's trajectory and the influence of the Púnguè and Buzi rivers and Urema Lake whose basins are locally considered as wetlands [65,66]. In this region we found a mixed spatial

distribution of the land cover, which mainly includes dense vegetation, agricultural land, and wetland along the coastline. The Southern region is characterized by abundant shrub land and a mixed vegetation distribution pattern including wetland vegetation, dense vegetation, and agriculture land which were all strongly affected by Cyclone Idai. To the south, the Save River, constituting the southern border of the Sofala Province, forms an estuary that is also considered wetland [63]. Li et al. [62] reported particularly significant levels of land degradation in the south-eastern region of the province, which could explain the more reduced agricultural land coverage we observed in this region.

#### 4.2. Effects of Idai on Different LULC

The changes in the different land-cover classes were calculated and compared with published literature. Dense vegetation (decreased by 58.9%), wetland vegetation (−57.4%) and shrub land (−55.5%) were among the most devastated vegetation classes, while barren land (−22.5%), barren vegetation (−26.9%) and grassland and dambos (−27.1%) were the least affected. From a biological perspective, our results show that the intensity of damage to different vegetation classes is closely related to their physiognomy. Dense vegetation, wetland vegetation, and shrub land are more vulnerable to physical damage by a tropical cyclone than the barren areas and herbaceous or sparse vegetation because of the higher tree layer and greater tree canopy cover. Numerous studies reported that forest stands with older and bigger trees (height, diameter and canopy) are more prone to wind damage than open, short and sparse forest stands [67–69]. An intense tropical cyclone like Idai typically causes great defoliation, branch stripping, bole snapping and uprooting [70–72]. Other individual tree characteristics, such as less dense wood, poor health status, and growth in more exposed sites (e.g., coastal Sofala, as shown by Cabral et al. [11] and Charrua et al. [10]), contribute to increasing its vulnerability to cyclone-related damage [70,73]. Other factors, such as the size of each LULC area, need to be deeply investigated. Rossi et al. [74] reported greater damage in larger forests in Northern Nicaragua as a result of hurricane Felix (2007). Generally, the spatial distribution of severe post-Cyclone Idai damage in Sofala closely matched the spatial distribution of the most devastated LULC. The damage behavior shown in different LULC in our study is consistent with other findings [23,24,70,73].

#### 4.3. The Influence of Distance on Damage

Our results demonstrate a strong positive correlation between distance and damage. The greatest damage in NDVI was found at distances shorter than 75 km (NDVI% from −52.29 to −55.07, Table 5), in accordance with previous studies [16,23,75]. The Pearson Correlation Coefficient between NDVI% and distance was 0.95 and R-square was 0.91, indicating a strong positive linear correlation (Figure 7). The spatial distribution of highly damaged regions across the Sofala Province (Figure 4) and the distance to Idai's trajectory suggest that the degree of damage does not entirely depend on the latter and that other factors may interfere, like the LULC type (vegetation physiognomy) [74,76].

Although this was not a ground data-based study because of the well-known difficulties of field research (e.g., time-consuming, limited availability of human and logistic resources), our results are realistic and they were satisfactorily verified with the local damage reports [12]. In fact, Landsat image analyses provided reliable results, and have been widely and successfully used to map LULC damages from cyclones [16,24,27,77]. This study can be employed as a future reference in related studies. Our approach clearly identified changes between pre- and post-cyclone LULC in Sofala; moreover, we found a strong correlation between the degree of damage and the distance from Idai's trajectory. Nevertheless, further studies are needed to quantify the local/regional changes that did not fit the linear model.



## 5. Conclusions

This study focuses on an analysis of the damage caused to the LULC by Cyclone Idai, which hit Sofala Province in Mozambique in March 2019. For that purpose, we used Landsat 7 and Landsat 8 images taken during the month of April over an 8-year period (2012–2019). All of the LULC classified areas showed a decrease of NDVI after the cyclone. The greatest damage was found in dense vegetation, wetland vegetation, and shrub land; barren land, barren vegetation, and grassland and dambos showed the lowest relative damage. The most heavily affected regions were the Northeast, Central and Southern Sofala. The distance to Idai's trajectory greatly influenced LULC damage levels—the greater the distance, the lower the damage. Besides the distance to Idai's trajectory, other factors such as LULC type (vegetation physiognomy) may have played an important role in terms of vegetation damage. The information here provided is relevant for LULC managers and all stakeholders to take appropriate measures for better planning and future management of the territory. In addition, our findings may help to speed up ongoing recovery processes that were activated in the wake of tropical Cyclone Idai.

**Author Contributions:** Conceptualization, A.B.C. and M.M.R.; methodology, A.B.C., R.P. and P.C.; formal analysis, A.B.C. and R.P.; investigation, A.B.C.; writing—original draft preparation, A.B.C.; writing—review and editing, A.B.C., R.P., P.C., S.B. and M.M.R.; supervision, P.C. and M.M.R. All authors have read and agreed to the published version of the manuscript.

**Funding:** This research was funded by Fundação para a Ciência e Tecnologia (FCT) of the Portuguese Government through the grants to A.C. (SFRB/BD/135360/2017), and research units UID/AGR/04129/2020-Linking Landscape, Environment, Agriculture and Food (LEAF) and UIDB/04152/2020-Centro de Investigação em Gestão de Informação (MagIC).

**Data Availability Statement:** Publicly available datasets were analyzed in this study. This data can be found here: <https://earthexplorer.usgs.gov>.

**Acknowledgments:** The authors would like to acknowledge the financial support provided by the Fundação para a Ciência e Tecnologia (FCT).

**Conflicts of Interest:** The authors declare no conflict of interest.

## References

1. Alam, E.; Dominey-Howes, D. A new catalogue of tropical cyclones of the northern Bay of Bengal and the distribution and effects of selected landfalling events in Bangladesh. *Int. J. Clim.* **2015**, *35*, 801–835. [\[CrossRef\]](#)
2. Tonkin, H.; Landsea, C.; Holland, G.J.; Li, S. Tropical cyclones and climate change: A preliminary assessment. In *Assessing Climate Change: Results from the Model Evaluation Consortium for Climate Assessment*; Howe, W., Henderson-Sellers, A., Eds.; Gordon and Breach: London, UK, 1997; pp. 327–360.
3. Lee, J.; Im, J.; Cha, D.H.; Park, H.; Sim, S. Tropical cyclone intensity estimation using multi-dimensional convolutional neural networks from geostationary satellite data. *Remote Sens.* **2020**, *12*, 108. [\[CrossRef\]](#)
4. Gray, W.M. Global View of the Origin of Tropical Disturbances and Storms. *Mon. Weather Rev.* **1968**, *96*, 669–700. [\[CrossRef\]](#)
5. Henderson-Sellers, A.; Zhang, H.; Berz, G.; Emanuel, K.; Gray, W.; Landsea, C.; Holland, G.; Lighthill, J.; Shieh, S.-L.; Webster, P.; et al. Tropical Cyclones and Global Climate Change: A Post-IPCC Assessment. *Bull. Am. Meteorol. Soc.* **1998**, *79*, 19–38. [\[CrossRef\]](#)
6. MICOA. *Avaliação da Vulnerabilidade as Mudanças Climáticas e Estratégias de Adaptação*; Ministry of Environment, Government of Mozambique: Maputo, Mozambique, 2005.
7. Consultec. *Estudo Ambiental Simplificado da Dragagem do Canal de Acesso ao Porto da Beira*; Consultec Consultores Associados Ltd.: Maputo, Mozambique, 2007.
8. Mavume, A.; Rydberg, L.; Rouault, M.; Lutjeharms, J. Climatology and Landfall of Tropical Cyclones in the South- West Indian Ocean. *West. Indian Ocean J. Mar. Sci.* **2009**, *8*, 15–36. [\[CrossRef\]](#)
9. Asante, K.; Brito, R.; Brundrit, G.; Epstein, P.; Fernandes, A.; Marques, M.R.; Mavume, A.; Metzger, M.; Nussbaumer, P.; Patt, A.; et al. *National Institute for Disaster Management Study on the Impact of Climate Change on Disaster Risk in Mozambique: Synthesis Report Acknowledgements*; Ministry of State Administration, Government of Mozambique: Maputo, Mozambique, 2009.
10. Charrua, A.B.; Bandeira, S.O.; Catarino, S.; Cabral, P.; Romeiras, M.M. Assessment of the vulnerability of coastal mangrove ecosystems in Mozambique. *Ocean Coast. Manag.* **2020**, *189*, 105145. [\[CrossRef\]](#)
11. Cabral, P.; Augusto, G.; Akande, A.; Costa, A.; Amade, N.; Niquisse, S.; Atumane, A.; Cuna, A.; Kazemi, K.; Mlucasse, R.; et al. Assessing Mozambique's exposure to coastal climate hazards and erosion. *Int. J. Disaster Risk Reduct.* **2017**, *23*, 45–52. [\[CrossRef\]](#)

12. Post Cyclone Idai Cabinet for Reconstruction. *Mozambique Cyclone Idai Post Disaster Needs Assessment*; Government of Mozambique: Beira, Mozambique, 2019.
13. UEM; FEWS; INGC. *Atlas For Deaster Preparedness and Response in the Limpopo Basin*; Government of Mozambique: Maputo, Mozambique, 2003.
14. Kolstad, E.W. Prediction and precursors of Idai and 38 other tropical cyclones and storms in the Mozambique Channel. *Q. J. R. Meteorol. Soc.* **2020**, 1–13. [[CrossRef](#)]
15. Salih, A.A.M.; Baraibar, M.; Mwangi, K.K.; Artan, G. Climate change and locust outbreak in East Africa. *Nat. Clim. Chang.* **2020**, 10, 584–585. [[CrossRef](#)]
16. Zhang, C.; Durgan, S.D.; Lagomasino, D. Modeling risk of mangroves to tropical cyclones: A case study of Hurricane Irma. *Estuar. Coast. Shelf Sci.* **2019**, 224, 108–116. [[CrossRef](#)]
17. Taillie, P.J.; Roman-Cuesta, R.; Lagomasino, D.; Cifuentes-Jara, M.; Fatoyinbo, T.; Ott, L.E.; Poulter, B. Widespread mangrove damage resulting from the 2017 Atlantic mega hurricane season. *Environ. Res. Lett.* **2020**, 15. [[CrossRef](#)]
18. Paling, E.I.; Kobryn, H.T.; Humphreys, G. Assessing the extent of mangrove change caused by Cyclone Vance in the eastern Exmouth Gulf, northwestern Australia. *Estuar. Coast. Shelf Sci.* **2008**, 77, 603–613. [[CrossRef](#)]
19. Bhowmik, A.K.; Cabral, P. Cyclone Sidr impacts on the Sundarbans floristic diversity. *Earth Sci. Res.* **2013**, 2, 62–79. [[CrossRef](#)]
20. Macamo, C.C.F.; Massuanganhe, E.; Nicolau, D.K.; Bandeira, S.O.; Adams, J.B. Mangrove's response to cyclone Eline (2000): What is happening 14 years later. *Aquat. Bot.* **2016**, 134, 10–17. [[CrossRef](#)]
21. Massuanganhe, E.A.; Macamo, C.; Westerberg, L.O.; Bandeira, S.; Mavume, A.; Ribeiro, E. Deltaic coasts under climate-related catastrophic events—Insights from the Save River delta, Mozambique. *Ocean Coast. Manag.* **2015**, 116, 331–340. [[CrossRef](#)]
22. Hoque, A.-A.M.; Phinn, S.; Roelfsema, C.; Childs, I.R. Assessing tropical cyclone impacts using object-based moderate spatial resolution image analysis: A case study in Bangladesh. *Int. J. Remote Sens.* **2016**, 37, 5320–5343. [[CrossRef](#)]
23. Hu, T.; Smith, R.S. The Impact of Hurricane Maria on the Vegetation of Dominica and Puerto Rico Using Multispectral Remote Sensing. *Remote Sens.* **2018**, 10, 827. [[CrossRef](#)]
24. Zhang, X.; Wang, Y.; Jiang, H.; Wang, X. Remote-sensing assessment of forest damage by Typhoon Saomai and its related factors at landscape scale. *Int. J. Remote Sens.* **2013**, 34, 7874–7886. [[CrossRef](#)]
25. Ballanti, L.; Byrd, K.B.; Woo, I.; Ellings, C. Remote sensing for wetland mapping and historical change detection at the Nisqually River Delta. *Sustainability* **2017**, 9, 1919. [[CrossRef](#)]
26. Li, D.; Lu, D.; Wu, M.; Shao, X.; Wei, J. Examining land cover and greenness dynamics in Hangzhou Bay in 1985–2016 using Landsat time-series data. *Remote Sens.* **2018**, 10, 32. [[CrossRef](#)]
27. Hu, L.; Li, W.; Xu, B. Monitoring mangrove forest change in China from 1990 to 2015 using Landsat-derived spectral-temporal variability metrics. *Int. J. Appl. Earth Obs. Geoinf.* **2018**, 73, 88–98. [[CrossRef](#)]
28. Schneibel, A.; Stellmes, M.; Röder, A.; Frantz, D.; Kowalski, B.; Haß, E.; Hill, J. Assessment of spatio-temporal changes of smallholder cultivation patterns in the Angolan Miombo belt using segmentation of Landsat time series. *Remote Sens. Environ.* **2017**, 195, 118–129. [[CrossRef](#)]
29. He, Y.; Yang, J.; Guo, X. Green Vegetation Cover Dynamics in a Heterogeneous Grassland: Spectral Unmixing of Landsat Time Series from 1999 to 2014. *Remote Sens.* **2020**, 12, 3826. [[CrossRef](#)]
30. Millennium Ecosystem Assessment. *Ecosystems and Human Well-Being: Synthesis*; Island Press: Washington, DC, USA, 2005.
31. INE. *IV Recenseamento Geral da População e Habitação 2017—Resultados Definitivos*; National Institute of Statistics, Government of Mozambique: Maputo, Mozambique, 2019.
32. Hogue, A.M. Perfil Diagnóstico da Zona Costeira de Moçambique. *Rev. Gest. Costeira Integr.* **2007**, 7, 69–82. [[CrossRef](#)]
33. Marzoli, A. *Avaliação Integrada de Florestas em Moçambique—Inventário Florestal Nacional*; Ministry of Agriculture, Government of Mozambique: Maputo, Mozambique, 2007.
34. Macamo, C.; Bandeira, S.; Muando, S.; Abreu, D.; Mabilana, H. Mangroves of Mozambique. In *Mangroves of the Western Indian Ocean: Status and Management*; Bosire, J.O., Mangora, M.M., Bandeira, S.O., Rajkaran, A., Appadoo, C., Kairo, J.G., Eds.; WIOMSA: Zanzibar Town, Tanzania, 2016; pp. 51–73. ISBN 9987955940.
35. Jensen, J.R. *Introductory Digital Image Processing: A Remote Sensing Perspective*, 2nd ed.; Prentice Hall: Upper Saddle River, NJ, USA, 2005.
36. Padmanaban, R.; Bhowmik, A.K.; Cabral, P. A remote sensing approach to environmental monitoring in a reclaimed mine area. *ISPRS Int. J. Geo Inf.* **2017**, 6, 401. [[CrossRef](#)]
37. Chen, J.; Zhu, X.; Vogelmann, J.E.; Gao, F.; Jin, S. A simple and effective method for filling gaps in Landsat ETM+ SLC-off images. *Remote Sens. Environ.* **2011**, 115, 1053–1064. [[CrossRef](#)]
38. Goslee, S.C. Analyzing Remote Sensing Data in R: The landsat Package. *J. Stat. Softw.* **2011**, 43, 1–25. [[CrossRef](#)]
39. Hossain, M.S.; Bujang, J.S.; Zakaria, M.H.; Hashim, M. Assessment of Landsat 7 Scan Line Corrector-off data gap-filling methods for seagrass distribution mapping. *Int. J. Remote Sens.* **2015**, 36, 1188–1215. [[CrossRef](#)]
40. USGS. Preliminary Assessment of the Value of Landsat 7 ETM+ SLC-off Data. Available online: <https://www.usgs.gov/media/files/preliminary-assessment-value-landsat-7-etm-slc-data> (accessed on 25 November 2020).
41. USGS. Phase 2 Gap-Fill Algorithm: SLC-Off Gap-Filled Products Gap-Fill Algorithm Methodology. Available online: <https://landsat.usgs.gov/sites/default/files/documents/L7SLCGapFilledMethod.pdf> (accessed on 19 September 2020).

42. Chander, G.; Markham, B.L.; Helder, D.L. Summary of current radiometric calibration coefficients for Landsat MSS, TM, ETM+, and EO-1 ALI sensors. *Remote Sens. Environ.* **2009**, *113*, 893–903. [\[CrossRef\]](#)
43. Gupta, K.; Mukhopadhyay, A.; Giri, S.; Chanda, A.; Datta Majumdar, S.; Samanta, S.; Mitra, D.; Samal, R.N.; Pattnaik, A.K.; Hazra, S. An index for discrimination of mangroves from non-mangroves using LANDSAT 8 OLI imagery. *MethodsX* **2018**, *5*, 1129–1139. [\[CrossRef\]](#)
44. Pathak, V.N.; Patel, K.D.; Trevedi, H.J. *Development of an Atmospheric Correction Method for Retrieval of Surface Reflectance from Satellite Data*; Sardar Patel University: Gujarat, India, 2016.
45. Leutner, B.; Horning, N.; Schwalb-Willmann, J. Stoolbox: Tools for Remote Sensing Data Analysis. R Package Version 0.2.6. Available online: <https://cran.r-project.org/web/packages/RStoolbox/index.html> (accessed on 18 September 2020).
46. Li, W.; El-askary, H.; Qurban, M.A.; Li, J.; Manikandan, K.P.; Piechota, T. Using multi-indices approach to quantify mangrove changes over the Western Arabian Gulf along Saudi Arabia coast. *Ecol. Indic.* **2019**, *102*, 734–745. [\[CrossRef\]](#)
47. Louarn, M.L.; Clergeau, P.; Briche, E.; Deschamps-Cottin, M. “Kill two birds with one stone”: Urban tree species classification using Bi-Temporal pléiades images to study nesting preferences of an invasive bird. *Remote Sens.* **2017**, *9*, 916. [\[CrossRef\]](#)
48. Padmanaban, R.; Bhowmik, A.K.; Cabral, P.; Zamyatin, A.; Almegdadi, O.; Wang, S. Modelling urban sprawl using remotely sensed data: A case study of Chennai city, Tamilnadu. *Entropy* **2017**, *19*, 163. [\[CrossRef\]](#)
49. Liaw, A.; Wiener, M. Classification and regression by randomForest. *R News* **2002**, *2*, 18–22.
50. R Core Team. A Language and Environment for Statistical Computing; R Foundation for Statistical Computing, Viena, Austria. Available online: <https://rstudio.com/products/rstudio/> (accessed on 16 September 2020).
51. Bivand, R.S.; Pebesma, E.J.; Gómez-Rubio, V. *Applied Spatial Data Analysis with R*; Springer International Publishing: Berlin, Germany, 2008; Volume 65, ISBN 978-0-387-78170-9.
52. Hijmans, R.J. Raster: Geographic Data Analysis and Modeling: R Package Version 3.3-13. Available online: <https://cran.r-project.org/web/packages/raster/index.html> (accessed on 16 September 2020).
53. Bivand, R.; Keitt, T.H.; Rowlingson, B. Rgdal: Bindings for the Geospatial Data Abstraction Library. R Package Version 1.5-16. Available online: <http://cran.r-project.org/%0Apackage=rgdal> (accessed on 25 September 2020).
54. Assal, T.J.; Anderson, P.J.; Sibold, J. Mapping forest functional type in a forest-shrubland ecotone using SPOT imagery and predictive habitat distribution modelling. *Remote Sens. Lett.* **2015**, *6*, 755–764. [\[CrossRef\]](#)
55. Walston, L.J.; Cantwell, B.L.; Krummel, J.R. Quantifying spatiotemporal changes in a sagebrush ecosystem in relation to energy development. *Ecography* **2009**, *32*, 943–952. [\[CrossRef\]](#)
56. Cakir, H.I.; Khorram, S.; Nelson, S.A.C. Correspondence analysis for detecting land cover change. *Remote Sens. Environ.* **2006**, *102*, 306–317. [\[CrossRef\]](#)
57. Naimi, B. rts: Raster Time Series Analysis: R Package Version 1.0-49. Available online: <https://cran.r-project.org/web/packages/rts/index.html> (accessed on 9 October 2020).
58. Zhu, Z.; Woodcock, C.E. Continuous change detection and classification of land cover using all available Landsat data. *Remote Sens. Environ.* **2014**, *144*, 152–171. [\[CrossRef\]](#)
59. Amone-Mabuto, M.; Bandeira, S.; Silva, A. Long-term changes in seagrass coverage and potential links to climate-related factors: The case of Inhambane Bay, southern Mozambique. *WIO J. Mar. Sci.* **2017**, *16*, 13–25.
60. Silva, J.A.; Sedano, F.; Flanagan, S.; Ombe, Z.A.; Machoco, R.; Meque, C.H.; Siteo, A.; Ribeiro, N.; Anderson, K.; Baule, S.; et al. Charcoal-related forest degradation dynamics in dry African woodlands: Evidence from Mozambique. *Appl. Geogr.* **2019**, *107*, 72–81. [\[CrossRef\]](#)
61. Devi, S. Cyclone Idai: 1 month later, devastation persists. *Lancet* **2019**, *393*, 1585. [\[CrossRef\]](#)
62. Li, Z.; Wang, S.; Song, S.; Wang, Y.; Musakwa, W. Detecting land degradation in Southern Africa using Time Series Segment and Residual Trend (TSS-RESTREND). *J. Arid Environ.* **2021**, *184*. [\[CrossRef\]](#)
63. Couto, A.; Bonate, P.; Simango, Y. *Inventário de Terras Húmidas em Moçambique: Identificação de Áreas com 500 Hectares ou Mais*; WWF and Biofund: Maputo, Mozambique, 2019.
64. Ramsar. Mozambique’s Zambezi Delta Extended to Cover 3000 Square Kilometres. Available online: <https://www.ramsar.org/news/mozambiques-zambezi-delta-extended-to-cover-3000-square-kilometres> (accessed on 3 November 2020).
65. Chabwela, H.N. Wetlands: A Conservation Programme for Southern Africa. A Report Document. In Proceedings of the IUCN, Wetlands Conservation Programme Southern African Development Coordination Conference, Gaborone, Botswana, 3–5 June 1991.
66. Saket, M. *Report on the Updating of the Exploratory National Forest Inventory*; Government of Mozambique: Maputo, Mozambique, 1994.
67. Gardiner, B.; Byrne, K.; Hale, S.; Kamimura, K.; Mitchell, S.J.; Peltola, H.; Ruel, J.C. A Review of Mechanistic Modeling of Wind Damage Risk to Forests. *Forestry* **2008**, *81*, 447–463. [\[CrossRef\]](#)
68. Lanquaye-Opoku, N.; Mitchell, S.J. Portability of Stand-Level Empirical Windthrow Risk Models. *For. Ecol. Manag.* **2005**, *216*, 134–148. [\[CrossRef\]](#)
69. Macisaac, D.A.; Krygier, R. Development and Long-Term Evaluation of Harvesting Patterns to Reduce Windthrow Risk of Understorey Spruce in Aspen-White Spruce Mixed Wood Stands in Alberta, Canada. *Forestry* **2009**, *82*, 323–342. [\[CrossRef\]](#)
70. Everham, E.M.; Brokaw, N.V. Forest damage and recovery from catastrophic wind. *Bot. Rev.* **1996**, *62*, 113–185. [\[CrossRef\]](#)

- 
71. Zimmerman, J.K.; Everham, E.M., III; Waide, R.B.; Lodge, D.J.; Taylor, C.M.; Brokaw, N.V.L. Responses of Tree Species to Hurricane Winds in Subtropical Wet Forest in Puerto Rico: Implications for Tropical Tree Life Histories. *J. Ecol.* **1994**, *82*, 911–922. [[CrossRef](#)]
  72. Lin, T.C.; Hogan, J.A.; Chang, C.-T. Tropical Cyclone Ecology: A Scale-Link Perspective. *Trends Ecol. Evol.* **2020**, *35*, 594–604. [[CrossRef](#)]
  73. Doyle, T.W.; Smith III, T.J.; Robblee, M.B. Wind damage effects of Hurricane Andrew on mangrove communities along the southwest coast of Florida, USA. *J. Coast. Res.* **1995**, *21*, 159–168. Available online: <https://www.jstor.org/stable/25736006> (accessed on 7 January 2021).
  74. Rossi, E.; Rogan, J.; Schneider, L. Mapping forest damage in northern Nicaragua after Hurricane Felix (2007) using MODIS enhanced vegetation index data. *GIScience Remote Sens.* **2013**, *50*, 385–399. [[CrossRef](#)]
  75. Doyle, T.W.; Girod, G.F.; Books, M.A. Modeling mangrove forest migration along the southwest coast of Florida under climate change. In *Integrated Assessment of the Climate Change Impacts on the Gulf Coast Region*; Ning, Z.H., Turner, R.E., Doyle, T.W., Abdollahi, K., Eds.; GCRCC: Baton Rouge, LA, USA, 2003; pp. 211–221.
  76. Foster, D.R.; Boose, E.R. Patterns of Forest Damage Resulting From Catastrophic Wind in Central New England, USA. *J. Ecol.* **1992**, *80*, 79–98. [[CrossRef](#)]
  77. Chamberlain, D.; Phinn, S.; Possingham, H. Remote sensing of mangroves and estuarine communities in central Queensland, Australia. *Remote Sens.* **2020**, *12*, 197. [[CrossRef](#)]